Simultaneous Landmark Classification, Localisation and Map Building for an Advanced Sonar Ring

Saeid Fazli and Lindsay Kleeman

(Saeid.fazli | Lindsay.kleeman)@eng.monash.edu.au

ARC Centre for Perceptive and Intelligent Machines in Complex Environments (PIMCE)

Intelligent Robotics Research Centre (IRRC)

Department of Electrical and Computer Systems Engineering

Monash University, Australia

Abstract

An autonomous mobile robot operating in an unknown indoor environment often needs to map the environment while localising within the map. Feature-based world models including line and point features are widely used by researchers. This paper presents a novel delayed classification algorithm to categorize these features using a recently developed high performance sonar ring within a Simultaneous Localisation And Map building (SLAM) process. The sonar ring sensor accurately measures range and bearing to multiple targets at near real time repetition rates of 11.5 Hz to 6 metres range and uses 24 simultaneously fired transmitters, 48 receivers and multiple echoes per receiver. The proposed algorithm is based on hypothesis generation and verification using the advanced sonar ring data and an Extended Kalman Filter (EKF) approach. It is capable of initiating new geometric features and classifying them within a short distance of travel of about 10 cm. For each new sonar reading not matching an existing feature, we initiate a pair of probational line and point features resulting from accurate range and bearing measurements. Later measurements are used to confirm or remove the probational features using EKF validation gates. The odometry error model of the filter allows for variations in effective wheel separation required by pneumatic robot tyres. The implementation of the novel classification and SLAM algorithm is discussed in this paper and experimental results using real sonar data are presented.
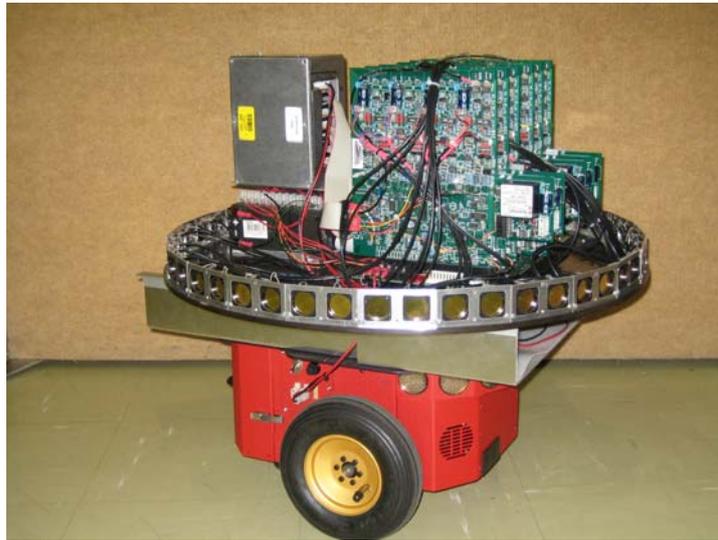
Fig. 1   The Robot *Sombrero.*

1. Introduction

Mapping is a fundamental requirement for a mobile robot to autonomously navigate in an *a priori* unknown indoor environment. The error growth of odometry dead-reckoning resulting from wheel distortion and slippage is usually unacceptable and environmental sensing is therefore needed. Building a map requires the interpretation of sensor information to estimate the locations of geometric features (landmarks) in a global reference map. This map is also used to determine the robot position in the environment. A large variety of sensor systems, such as sonar, radar, laser, infrared and vision are commonly used to make mobile robots capable of sensing their environment [1-7]. Also different world models such as feature-based and grid-based are widely used by researchers to map the environment [8-13]. To build a feature-based map, one has to decide what features to use to describe the robot's environment. Some researchers have used only line segments [14] and many researchers have built maps containing lines and points [2,15,16]. Cylinders and arcs are rarely included in the feature set [17]. All measurements of geometric features are contaminated with background noise, false targets and phantom targets. The crucial problem in using sensory information to generate a map is the uncertainty in the origin of measurements and uncertainty in the robot position. Stochastic mapping using EKF are widely used by researchers to solve this problem [7,11,15,16,18-20].

The other crucial problem for sonar sensors is to classify the sensor information to discriminate planes, corners and edges. This is important in terms of being able to predict the measurements from a new position and hence apply an update procedure such as the Kalman filter. Some researchers have developed sonar sensors which allow target classification at one position [16,21-23]. However, typical sonar sensors are commonly unable to classify the targets from one position because sonar observations are discrete points. Therefore, while navigating along a wall, the robot sees the wall not as a line but as a set of points. It is only through accumulation of observations over time that a correct feature

classification can be made and a map can be constructed. Delayed decision making techniques using Hough transforms are widely used by researchers to classify the landmarks [8,9,24-28].

This paper presents a novel classification method within the SLAM process. The proposed algorithm is based on delayed decision making using hypothesis generation and verification and accurate sonar data. The map considered in this work is feature-based and consists of natural landmarks that occur in indoor environments; planes, corners and edges modeled into lines and points. The work presented here is the first reported mapping results from a recently developed fast and accurate sonar ring [29] mounted on the robot *Sombrero* shown in Fig. 1 in real indoor environments. Confirmation, deletion and initiation of new geometric features and SLAM process using EKF are included in the algorithm. If a new sonar reading is not associated with current features, a pair of probational features (a line and a point) will be initiated. The point feature is initiated in the location of the observed target and the line feature, perpendicular to the line connecting the transmitter to the target. The validation gate condition of the Kalman filter is used to confirm or remove the probational features within the next 10 robot positions. Due to the high repetition rate of the advanced sonar ring of about 11.5 Hz, the confirmation and deletion process can be performed by the robot within 10 cm from where the feature is first sensed (or about 0.8 seconds at robot speeds of 10 cm/sec). The high speed classification helps to minimize the number of probational features and to speed up the mapping process. The odometry error model similar to the one of [16] is used in this work which incorporates variations in effective wheel separation and angle measurements. This model is suited to pneumatic tyre odometry errors where the wheel separation has been found to vary unpredictably with floor surface and path curvature. This paper also describes a novel sonar data filtering technique to eliminate many phantom targets due to multi-path echoes.

The paper is organised as follows: The next section contains an overview of the robot *Sombrero* and gives an overview of the software and hardware structure of the advanced sonar ring. Section 3 explains the details of the proposed landmark classification and SLAM approach. Section 4 presents implementation details of the algorithm. Experimental results are presented in Section 5 to show the effectiveness of the proposed algorithm. Conclusions and a discussion of future work form the last section of the paper.

2. Overview of the Mobile Robot *Sombrero*

The *Sombrero* consists of an advanced sonar ring sensor mounted on an ActivMedia Pioneer 3 DX mobile robot. Locomotion method of the Sombrero is differential drive and Powered Wheel Steering (PWS) mechanism is used to control the robot motion. The advanced sonar ring works by simultaneously firing of all transmitters and hence emitting a burst of ultrasound in all directions, and waiting for the echoes reflected from any objects within the sound beam. Then potential echo sample intervals are extracted from all 48 receivers using a thresholding method. These echo sample intervals are later processed on DSPs to obtain echo accurate arrival times.

To maximize the speed of the sensor and to be able to perform the task in the limited memory of the DSP memory, an interrupt service routine performs thresholding while receivers are listening to echoes. The delays, known as the Time-Of-Flight (TOF), are estimated for all the echoes reflected from different objects to every receiver in each firing. Then the calculated Distance-Of-Flight (DOF) of the returned echoes is twice the distance to the object. The bearing angle is determined by combining multiple measurements on different receivers. The basic idea is to calculate TOF for each receiver by means of matched filtering (also called template matching) which is the minimum variance arrival time estimator in the presence of additive white Gaussian noise on the echo. A matched filter is based on finding the peak of the cross correlation of the echo with an *a priori* calculated template. This technique has been extensively used in [15,21,22,30].

The Field of view of the Polaroid 7000 transducers used in the advanced sonar ring is about 15 degrees, therefore 24 pairs of transducers are considered to cover all around the robot and make it able to estimate the bearing using one transceiver and one receiver in every pair. Fig. 2 shows an overview of the hardware structure of the advanced sonar ring.
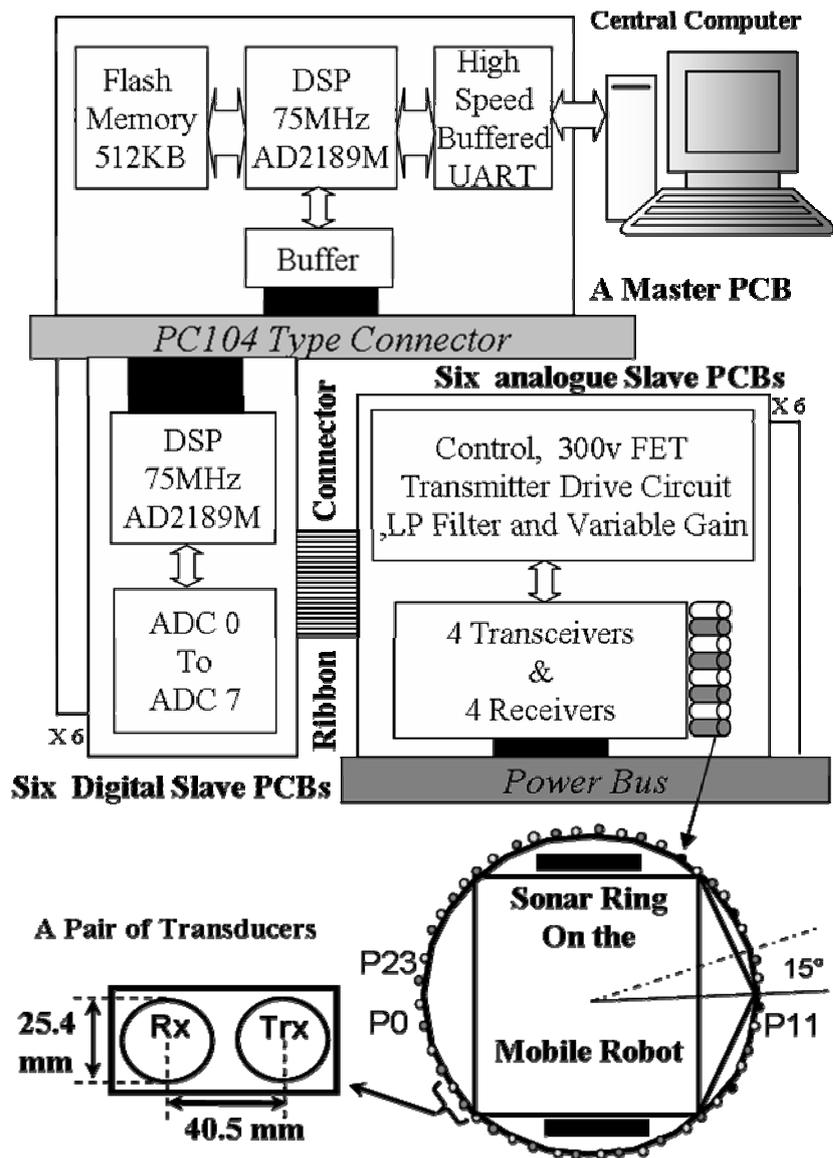
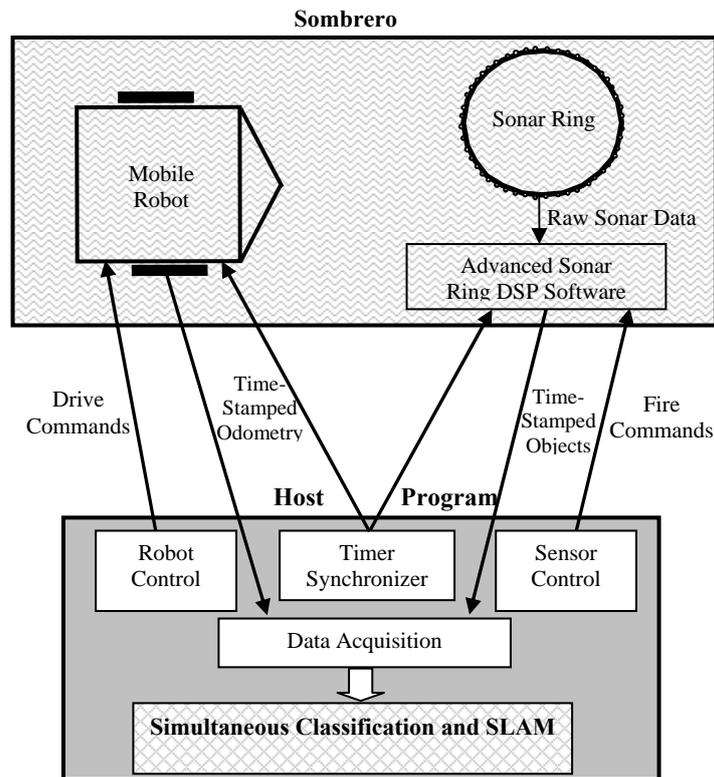**Fig. 2** The Block Diagram of the Advanced Sonar Ring Hardware.

Fig. 3 Overview of the Host Software of *Sombrero.*

Six DSP boards called slave PCBs are designed to manage all 48 transducers. Each DSP processes the echoes returned to eight receiver channels. Each slave board is responsible for controlling the transmission and data acquisition process for four pairs of transceiver and receivers, grouped into four pairs. Also the board contains a high voltage DC-DC converter to produce a 300 V bias on the 8 transducers.

Finally a master DSP is designed to communicate with all slave PCBs and to manage them. A master DSP also in turn relays results of all slaves to a host computer over a serial line. One of the advantages of this configuration is that it relieves the computational burden of the host computer allowing computationally intensive applications to take place on a moving platform. Fig. 3 shows an overview of the software structure of the host computer that controls the robot *Sombrero* and communicates with the sonar ring. The sonar ring can sense smooth targets, such as planes and right angled corners, with an accuracy of approximately 0.6 mm and 0.2 degrees for ranges from 0.2 to 4 metres [29].

3. Landmark Classification and SLAM for Autonomous Navigation

We assume that the actual three dimensional world model is orthogonal to the horizontal plane of the sonar ring, so the environment can be adequately represented by a two dimensional map. A stochastic feature-based mapping method based on EKF is used for simultaneously localisation of *Sombrero* and mapping of the environment. The method is based on the description by Davison [6] where all map features are updated on each measurement result. In each robot pose only one set of sensor results are applied to SLAM in order to speed up the process. This means if multiple firings

occur in the same robot pose, the results of the first firing are applied to the algorithm and the rest are ignored. In the following subsections 3.1 and 3.2 a vehicle model and its associated errors is developed that allows odometry inputs to predict the motion of the robot. The Kalman filter facilitates the fusion of these odometry inputs with sonar measurements (discussed in subsection 3.3) by predicting environmental features (discussed in subsection 3.4) and correcting them using an error model of the sonar measurements as described in subsection 3.5. Subsection 3.6 describes how sonar features are classified and integrated into the map building processing.

3.1 Mobile Vehicle Model

The robot state vector is denoted as:

$$\mathbf{x}_R = [\theta \quad x \quad y]^T \tag{1}$$

comprising a heading and the Cartesian location of the centre of the drive wheel axis defined with respect to the global coordinate frame shown in Fig. 4. The state vector of the robot is initialised to $[0 \quad 0 \quad 0]^T$.

Internal sensors (encoders) give information about the speed and distance the robot wheels move. This information must be integrated to give the robot's global position and direction. On *Sombrero* the encoder counts are accumulated for 20 ms, and then used to update the position of the robot. Based on the encoder counts of the wheel, distance moved by each wheel is estimated. Therefore, at the end of 20 ms the right wheel has traveled a distance Δr, and the left wheel Δl.

Fig. 4 shows the path of the robot when it moves to a new position. The combined rotation and translation motion is shown in the figure. We assume that the robot travels in an arc while it translates a distance Δs and turns an angle $\Delta \theta$. By using the notation of Fig. 4, the distances traveled can be expressed as:

$$\begin{cases} \Delta l = \Delta \theta . R \\ \Delta r = \Delta \theta . (R + B) \end{cases} \tag{2}$$

and therefore:

$$\begin{cases} \Delta \theta = (\Delta r - \Delta l) / B \\ R = (\Delta l . B) / (\Delta r - \Delta l) \end{cases} \tag{3}$$
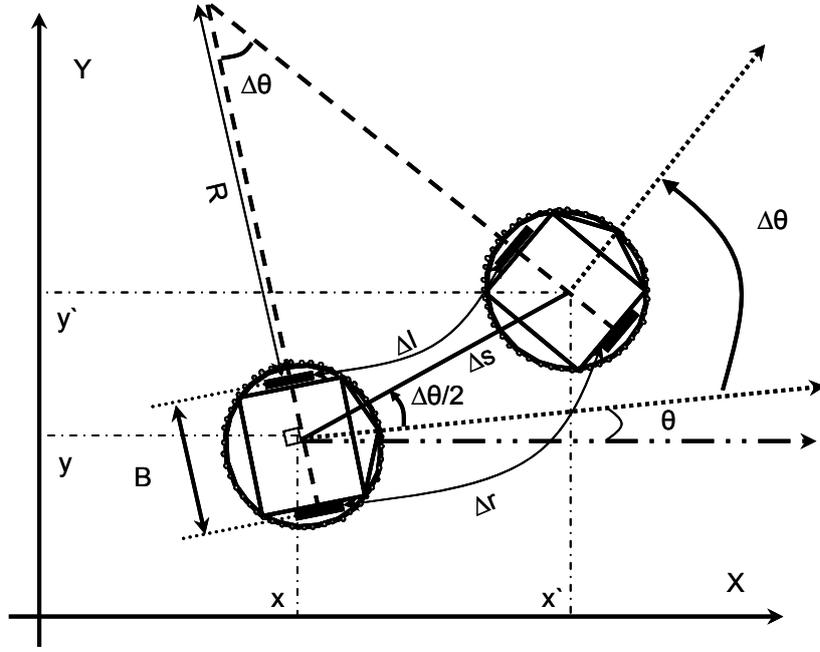
Fig. 4   Geometry of the Robot Movement.

From the Law of Cosines:

$$\Delta s^2 = 2.(R + B/2)^2 - 2.(R + B/2)^2.\cos(\Delta\theta) \tag{4}$$

Using equation (3), Δs can be rewritten as:

$$\Delta s = \frac{B.(\Delta r + \Delta l)}{(\Delta r - \Delta l)}.\sin(\Delta\theta/2) \overset{\Delta\theta \to 0}{\approx} (\Delta r + \Delta l)/2 \tag{5}$$

It can be proved that the angle between the translation vector (Δs) and the heading of the robot is $\Delta\theta/2$ as shown in Fig. 4. Therefore, if in the next time increment the robot moves a distance Δs and turns $\Delta\theta$, then the new position of the robot $[\theta' \quad x' \quad y']^T$ can be calculated as:

$$\begin{cases} \theta' = \theta + \Delta\theta \\ x' = x + \Delta s.\cos(\theta + \Delta\theta/2) \\ y' = y + \Delta s.\sin(\theta + \Delta\theta/2) \end{cases} \tag{6}$$

3.2. The Odometry Error Propagation under Robot Motion

We denote the robot state vector at time step k by the vector $\mathbf{x}_R(k) = [\theta(k) \quad x(k) \quad y(k)]^T$. Using equations (3-6), the robot's motion through the environment is described as:

8

$$\mathbf{x}_R(k+1) = \mathbf{x}_R(k) + \mathbf{f}(\mathbf{x}_R(k), \mathbf{y}(k))$$

$$\mathbf{y}(k) = [\Delta r \quad \Delta l \quad B]^T \tag{7}$$

$$\mathbf{f}(\mathbf{x}_R(k), \mathbf{y}(k)) = \begin{bmatrix} (\Delta r - \Delta l)/B \\ \dfrac{\Delta r + \Delta l}{2} \cos(\theta(k) + \dfrac{\Delta r - \Delta l}{2.B}) \\ \dfrac{\Delta r + \Delta l}{2} \sin(\theta(k) + \dfrac{\Delta r - \Delta l}{2.B}) \end{bmatrix}$$

As the robot moves, the odometry errors accumulate to make the robot's overall position very uncertain with respect to the global frame. This uncertainty is produced by two mechanisms: the addition of new position integration errors and the development of previous errors under motion. The error model explained in this section which is similar to [16], considers noise on Δr, Δl and B. *Sombrero* has inflatable tyres that provide good traction at the expense of wheel separation uncertainty. Using a first order Taylor expansion of equations (7) the iterative equation can be derived in terms of the Jacobians $\dfrac{\partial \mathbf{f}}{\partial \mathbf{x}}$ and $\dfrac{\partial \mathbf{f}}{\partial \mathbf{y}}$ (see [16] for more details):

$$\Delta \mathbf{x}_R(k+1) \cong (\mathbf{I} + \frac{\partial \mathbf{f}}{\partial \mathbf{x}}) \Delta \mathbf{x}_R(k) + \frac{\partial \mathbf{f}}{\partial \mathbf{y}} \Delta \mathbf{y}(k) \tag{8}$$

The covariance of the error in the robot pose at step $k+1$ is now derived in terms of step k:

$$
\begin{aligned}
\mathbf{P}_{RR}(k+1) &\equiv E\left\langle \Delta \mathbf{x}_R(k+1) \Delta \mathbf{x}_R(k+1)^T \right\rangle \\
&= (\mathbf{I} + \frac{\partial \mathbf{f}}{\partial \mathbf{x}_R}) E\left\langle \Delta \mathbf{x}_R(k) \Delta \mathbf{x}_R(k)^T \right\rangle (\mathbf{I} + \frac{\partial \mathbf{f}}{\partial \mathbf{x}_R})^T + \frac{\partial \mathbf{f}}{\partial \mathbf{y}} E\left\langle \Delta \mathbf{y}(k) \Delta \mathbf{y}(k)^T \right\rangle \frac{\partial \mathbf{f}}{\partial \mathbf{y}}^T \\
&= \underbrace{\mathbf{P}_{RR}(k) + \mathbf{P}_{RR}(k) \frac{\partial \mathbf{f}}{\partial \mathbf{x}_R}^T + \frac{\partial \mathbf{f}}{\partial \mathbf{x}_R} \mathbf{P}_{RR}(k) + \frac{\partial \mathbf{f}}{\partial \mathbf{x}_R} \mathbf{P}_{RR}(k) \frac{\partial \mathbf{f}}{\partial \mathbf{x}_R}^T}_{\mathrm{cov} \, ariance \; propagation} + \underbrace{\frac{\partial \mathbf{f}}{\partial \mathbf{y}} \mathbf{Q}(k) \frac{\partial \mathbf{f}}{\partial \mathbf{y}}^T}_{newerror}
\end{aligned} \tag{9}
$$

where E is expectation and $Q(k)$ is the error covariance of $y(k)$, the wheel measurements and separation. We assume that in equation (9), the errors in robot pose, x, at time k and the new errors in odometry parameters y at time k are independent. The errors in Δr, Δl and B are assumed to be independent:

$$\mathbf{Q} = \begin{bmatrix} \sigma_r^2 & 0 & 0 \\ 0 & \sigma_l^2 & 0 \\ 0 & 0 & \sigma_B^2 \end{bmatrix} \tag{10}$$

The covariance update equation (9) can be calculated in a computationally effective manner as explained in [16]. The values for the variances σ_r^2 and σ_l^2 must be proportional to Δr and Δl at each step to make the system consistent which means for a given range or angle change, the final covariance should be independent of the number of steps to traverse a path [16]. Since the covariances add when independent noise segments are concatenated, these covariances must be proportional to the distance traveled:

$$\begin{cases} \sigma_r{}^2 = E^2|\Delta r| \\ \sigma_l{}^2 = E^2|\Delta l| \end{cases} \tag{11}$$

where E is the error standard deviation for 1 metre travel. Also from [16] $\sigma_B{}^2$ can be written as:

$$\sigma_B{}^2 = \frac{A^2 B^2}{2\pi|\Delta\theta|} \tag{12}$$

where A is the angle error standard deviation for a full 2π revolution of the robot in one step that is attributed to variations in the wheel separation B.

3.3. Geometric Feature Models

The environmental landmarks are modeled as lines and points. The lines represent plane reflectors while point features are used for corners and edges. The point feature is characterized by its two dimensional Cartesian coordinates $[x_p \quad y_p]^T$. The plane feature is represented by a line with an angle φ and the minimum distance d to the global coordinate system origin as shown in Fig. 5. The line $[\varphi \quad d]^T$ can be represented by a parametric equation:

$$\begin{cases} x = d\cos\varphi + t\sin\varphi \\ y = d\sin\varphi - t\cos\varphi \end{cases} \tag{13}$$
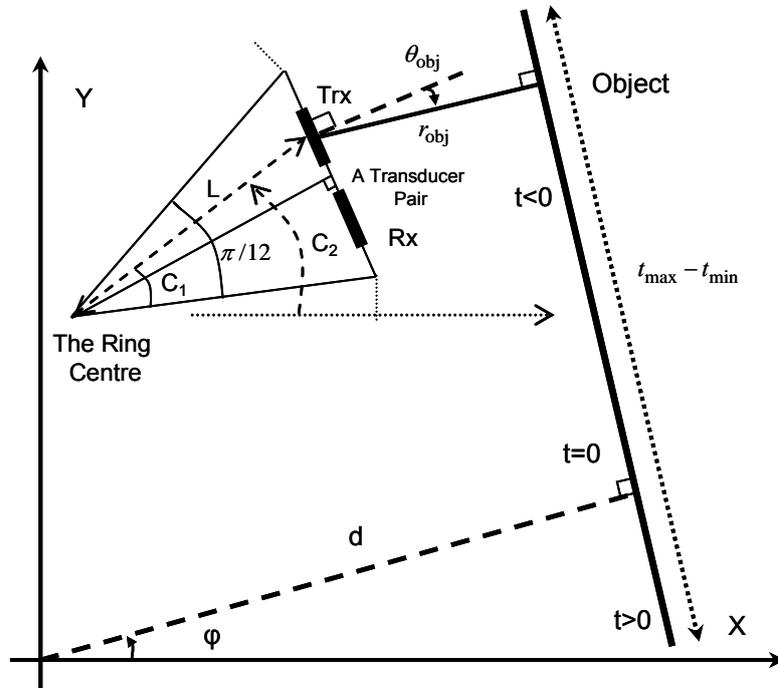

Fig. 5 Line Representation.

10

where the parameter t is the signed distance from the nearest point on the line to the origin. In order to model a partial plane, parameters t_{min} and t_{max} are saved to determine line endpoints. The length of the partial line is also represented by $t_{max} - t_{min}$. The parametric equation (13) can also be written as:

$$g(x, y) = y \sin \varphi + x \cos \varphi - d = 0 \tag{14}$$

The representation $[\varphi \quad d]^T$ has the alternative of $[\varphi + \pi \quad -d]^T$ that results in the same parametric equations except t reverses sign. Here the two lines are considered different since they correspond to sensing from different sides of the line. If the line were sensed from the other side of the coordinate origin, a negative distance parameter would be recorded. This representation differentiates between two sides of a partial plane. That means:

$$\begin{cases} if \left(sign(g(0,0)) == sign(g(trx_x, trx_y)) \right) \Rightarrow change \ d \ to \ positive \\ else \qquad\qquad\qquad\qquad\qquad\qquad \Rightarrow change \ d \ to \ negative \end{cases} \tag{15}$$

where (trx_x, trx_y) are the coordinates of the transceiver that observes the partial plane (Fig. 5). New sonar measurements are only fused with the line if their t parameter lies in the line or in the extension of the line by less than 0.2 m. When an extension of the line is accepted by the EKF as described by the validation gate of equation (41) below the values of t_{min} and t_{max} are updated.

3.4. Prediction of Geometric Feature Positions

The advanced sonar ring consists of 24 transducer pairs numbered from 0 to 23 (see Fig. 2). Each pair has a transceiver and a receiver. The sensor fires all transceivers simultaneously then the results of echo signal processing including the pair number that senses the reflector and the DOFs of the transducers are sent to the host program. This information is used to estimate the reflector state parameters as follows.
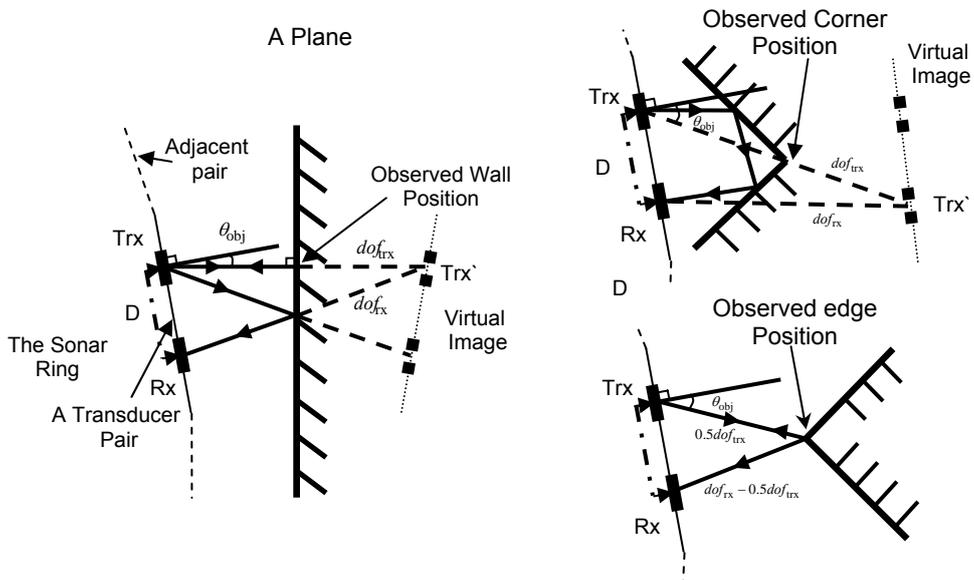

Fig. 6   The Geometry of Sensing a Plane, a Corner and an Edge.

11

The geometry of sensing a plane, a corner and an edge are shown in Fig. 6. The label *Trx* is used for a transceiver and *Rx* for a receiver. The DOFs are labeled dof_{trx} and dof_{rx}. Based on the geometry shown in Fig. 6, the incidence angle θ_{obj} can be calculated by applying the Law of Cosines:

$$\theta_{obj} = \begin{cases} \dfrac{\pi}{2} - \cos^{-1}\left(\dfrac{D^2 + dof_{trx}{}^2 - dof_{rx}{}^2}{2.D.dof_{trx}} \right) & \text{for a corner or a plane} \\[4mm] \dfrac{\pi}{2} - \cos^{-1}\left(\dfrac{D^2 + \left(0.5dof_{trx}\right)^2 - \left(dof_{rx} - 0.5dof_{trx}\right)^2}{2.D.\left(0.5dof_{trx}\right)} \right) & \text{for an edge} \end{cases} \tag{16}$$

where D is the separation between the transceivers of each pair. The distance of an object to a transceiver, r_{obj} is determined by:

$$r_{obj} = 0.5\,dof_{trx} \tag{17}$$

As the map primitives are lines and points and there is no differentiation between corners and edges, the first equation in (16) is used to calculate the bearing angle of the reflector. On the other hand, the sensor does not classify the objects at the first step therefore the application assumes that the reflector is a corner or a plane feature and uses the same equation for all sonar measurements. This assumption is acceptable because the difference in results of both equations in (16) is usually small. For example the difference is less than 0.4 degrees for ranges greater than 1.5 metres. When accuracy is important, a target classified as an edge can be adjusted in angle accordingly.

The coordinates of the transceiver that senses the object with respect to the global system is determined using the robot state $[\theta'\ x'\ y']^T$ and definitions shown in Fig. 5:

$$\begin{cases} Trx_x = x + L\cos(\theta + C_2) \\ Trx_y = y + L\sin(\theta + C_2) \\ C_2 \equiv \dfrac{\pi}{12}.pair_{no} + \pi + C_1 \end{cases} \tag{18}$$

where $pair_{no}$ is the sequence number of the transducer pair (P0 to P23 in Fig. 2). The parameters L, C_1 and C_2 are shown in Fig. 5 and are determined by the geometric design and construction of the sonar ring. The measured values of L and C_1, used in this work are 0.3083 metre and 0.1966 radian respectively.

Therefore, the position of the object can be written as:

$$\begin{cases} object_x = Trx_x + r_{obj}\cos(\theta - \theta_{obj} + C_3) \\ object_y = Trx_y + r_{obj}\sin(\theta - \theta_{obj} + C_3) \\ C_3 \equiv \dfrac{\pi}{12}.pair_{no} + \pi + \dfrac{\pi}{24} \end{cases} \tag{19}$$

If we assume that the measured reflector is a partial plane, then using equations (14), (18) and (19), we can calculate the parameters φ and d of the line feature that is perpendicular to the line between Trx and the object for the object position:

$$\begin{cases} \varphi = \tan^{-1}\left(\dfrac{object_y - trx_y}{object_x - trx_x} \right) \\ d = object_y \sin\varphi + object_x \cos\varphi \end{cases} \tag{20}$$

Equation (15) is then applied to achieve a consistent representation.

If we assume that the target is a point feature then the coordinates of the target can be used as the feature parameters and from equations (18) and (19):

$$\begin{cases} x_p = x + L\cos(\theta + C2) + r_{obj}\cos(\theta - \theta_{obj} + C_3) \\ y_p = y + L\sin(\theta + C2) + r_{obj}\sin(\theta - \theta_{obj} + C_3) \end{cases} \tag{21}$$

3.5. Measurement Model

At time step k, the robot obtains sonar measurements dof_{trx} and dof_{rx} from a pair of transducers. Then using equations (16) and (17), the measurement vector is formed:

$$\mathbf{z}(k) = [\theta_{obj}(radian) \quad r_{obj}(metre)]^T \tag{22}$$

On the other hand, the value of the measurement $\mathbf{z}(k)$ is a function of the robot state at time k and the location of the feature from which it originated, subject to a noise disturbance, as given by the measurement model:

$$\begin{cases} \mathbf{z}(k) = \mathbf{h}\big(k, \mathbf{x}(k)\big) + \mathbf{w}(k) \\ \mathbf{x}(k) = [\mathbf{x}_R(k) \quad \mathbf{x}_1(k) \quad ... \quad \mathbf{x}_n(k)]^T \end{cases} \tag{23}$$

where $x(k)$ is the system state vector including the robot state vector and all n geometric features. The measurement model, h, takes different forms depending on the type of feature, and w is the measurement noise with error covariance which is defined as:

$$\mathbf{R}(k) = E\big\langle \mathbf{w}(k)\mathbf{w}(k)^T \big\rangle = \begin{bmatrix} (2\,degree \times \dfrac{\pi}{180})^2 & 0 \\ 0 & (0.004\,metre)^2 \end{bmatrix} \tag{24}$$

To define the measurement model, h, of a plane reflector, we assume that the line state $[\varphi \quad d]$ is known. Then by using the robot state and $pair_{no}$ at time step k the measurement elements θ_{obj} and r_{obj} are calculated:

$$\begin{cases} \theta_{obj} = \theta - \varphi + C_3 \\ r_{obj} = \big|(x + L\cos(\theta + C_2))\cos\varphi + (y + L\sin(\theta + C_2))\sin\varphi - d\big| \end{cases} \tag{25}$$

13

To define measurement model $\boldsymbol{h}$ for a corner or an edge reflector, we assume that the point state $[x_p \ y_p]$ is known. Then by using the robot state and $pair_{no}$ at time step k the measurement elements θ_{obj} and r_{obj} are derived:

$$\begin{cases} \theta_{obj} = \theta + C_3 - \tan^{-1}\left(\dfrac{y_p - y - L\sin(\theta + C_2)}{x_p - x - L\cos(\theta + C_2)} \right) \\ r_{obj} = \sqrt{(x_p - x - L\cos(\theta + C_2))^2 + (y_p - y - L\sin(\theta + C_2))^2} \end{cases} \tag{26}$$

3.6. Proposed Classification and SLAM Algorithm

Accurate measurements of range and bearing angle are performed within the multi-DSP architecture of the advanced sonar ring as explained in Section 2. Each measurement introduces a dot in the world frame that can be part of a partial plane or the position of a corner (or an edge). The advantage of accurate bearing angles provided by the advanced sonar ring [29,31,32], is that it allows us to precisely calculate the state parameters of the predicted partial plane from each measurement result. The predicted plane feature is a line perpendicular to the line between the transmitter and the object in the object position. A predicted corner or edge feature is a point in the measured reflector position as explained in Section 3.4. This prediction of the object position from one sonar result is not possible for conventional sonar sensors due to a large uncertainty in the bearing angle. The proposed classification and SLAM algorithm uses an extended Kalman filter to update the robot position and the features' positions and also to classify the targets. It uses the method introduced by Davison [6] where all map features are updated on each measurement result. The method here differs from Davison [6] in the sensor employed (ie sonar ring) and the method for classifying the sonar targets as the robot moves, as described below. Fig. 7 shows a flow chart of the proposed classification and SLAM method that is detailed below.
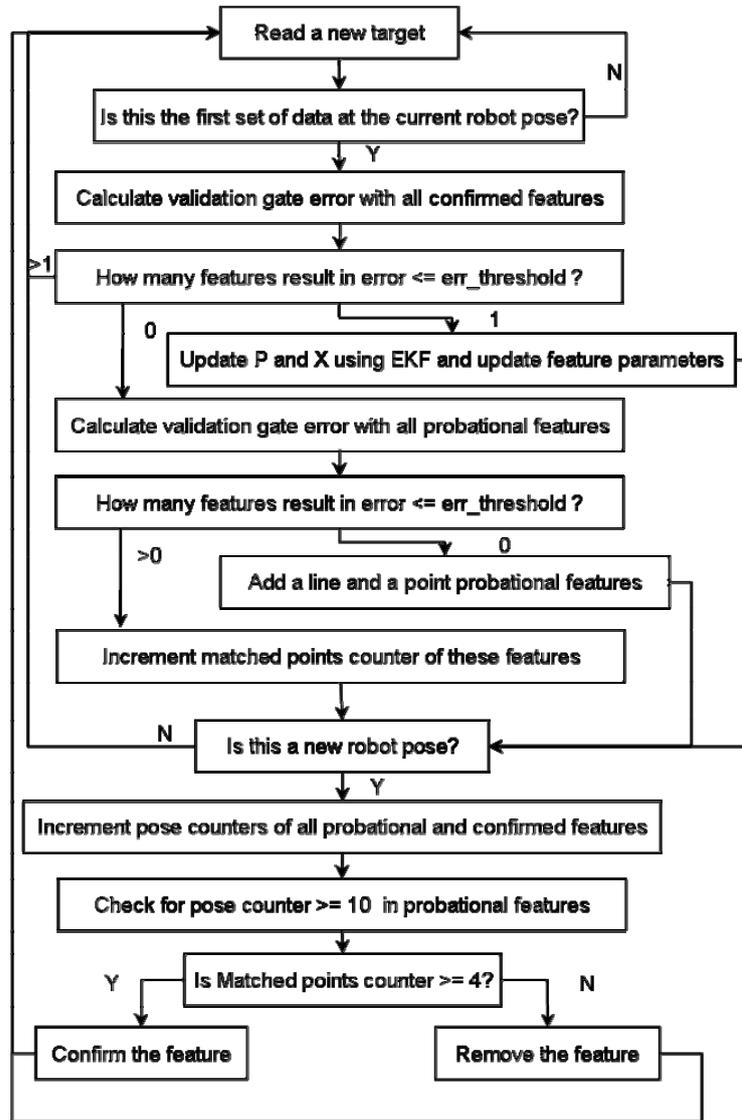
Fig. 7 The Block Diagram of the Proposed Classification and SLAM Algorithm. The *error* and *err_threshold* are explained just after equation (41) and relate to the validation gate of the Kalman filter. The "matched points counter" is incremented when a measurement falls in the validation gate.

Measurement to feature association plays an important role for both the classification and SLAM processes. In fact, data association (which feature a measurement is generated from), can significantly affect the map. The validation gate condition for a Kalman filter is used for data association. This is explained in detail in the next section. The new measurements can either generate new map features or be fused to existing features. After each association, all error covariance and cross covariance matrices are updated by the fusion of a new result.

The classification algorithm is based on multi-hypothesis generation and verification. If a new result is not associated with existing features, two probational features as hypotheses, are generated: a line and a point. The state parameters of these features are calculated from single measurement result as explained in Section 3.4. The robot inserts them into its probational feature matrix. The features are partitioned into probational and confirmed features, with only

the confirmed features used for SLAM. The verification is performed based on the association results on sensor measurements within the robot's next ten positions. The repetition rate of the sensor is 11.5Hz [29], therefore the verification process is performed within about 1 second when the robot is moving. The method is capable of initiation, confirmation and deletion of the geometric features. After confirmation, the feature is moved from probational to the confirmed partition and is used in the SLAM process.

4. Implementation Details

As explained in the previous sections, the robot state vector at time step k, $\mathbf{x}_R(k)$ and state vectors of the confirmed features $\mathbf{x}_i(k)$ comprise the system state vector $\mathbf{x}(k) = [\mathbf{x}_R(k) \ \mathbf{x}_1(k) \ ... \ \mathbf{x}_n(k)]^T$, where n is number of the confirmed features and $\mathbf{x}_i(k)$ is $[\varphi \ d]^T$ for line features and $[x_p \ y_p]^T$ for point features. The measurement model of the system, $z(k)$ is as defined in equation (23). The objective of the SLAM is to use the EKF to recursively compute an estimate for $\mathbf{x}(k)$:

$$\hat{\mathbf{x}}(k) = [\hat{\mathbf{x}}_R(k) \ \hat{\mathbf{x}}_1(k) \ ... \ \hat{\mathbf{x}}_n(k)]^T \tag{27}$$

which is called the system state estimate, and its covariance is called the system state prediction covariance matrix:

$$\mathbf{P}(k \mid k) = \begin{bmatrix} \mathbf{p}_{RR}(k \mid k) & \mathbf{p}_{R1}(k \mid k) & . & . & . & \mathbf{p}_{Rn}(k \mid k) \\ \mathbf{p}_{R1}(k \mid k) & \mathbf{p}_{11}(k \mid k) & . & . & . & \mathbf{p}_{1n}(k \mid k) \\ . & . & . & & . \\ . & . & . & . & . \\ . & . & . & . & . \\ \mathbf{p}_{Rn}(k \mid k) & \mathbf{p}_{1n}(k \mid k) & . & . & . & \mathbf{p}_{nn}(k \mid k) \end{bmatrix} \tag{28}$$

where $\mathbf{p}_{Ri}(k \mid k)$ is a robot to feature cross-covariance matrix at time step k given measurements $\mathbf{z}(k)$, $\mathbf{z}(k-1)$, ... , $\mathbf{p}_{ij}(k \mid k)$ is a feature to feature cross-covariance matrix and a covariance of error in the feature state is denoted as $\mathbf{p}_{ii}(k \mid k)$.

The EKF can be formulated into a two stage process:

1- System state prediction: $\hat{\mathbf{x}}(k+1 \mid k)$ - estimate of x at step $k+1$ given measurements $\mathbf{z}(k)$, $\mathbf{z}(k-1)$, ...

2- System state update: $\hat{\mathbf{x}}(k+1 \mid k+1)$ and $\mathbf{p}(k+1 \mid k+1)$

In order to perform the first stage, the system state is estimated which contains the robot position vector and all features states. Robot state prediction, $\hat{\mathbf{x}}_R(k+1 \mid k)$ is calculated using Δr and Δl, given by the odometry system as explained in Section 3.2, equation (7). The prediction of features states, $\hat{\mathbf{x}}_i(k+1 \mid k)$, due to assuming a stationary environment, is taken to be the same as $\hat{\mathbf{x}}_i(k \mid k)$.

16

Stage two of EKF can be divided into state estimation and state covariance estimation.

State estimation consists of:

- Measurement Prediction:

$$\hat{\mathbf{z}}(k+1\,|\,k) = \mathbf{h}\left(k+1, \hat{\mathbf{x}}(k+1\,|\,k)\right) \qquad (29)$$

- Measurement Residual:

$$\mathbf{v}(k+1) = \mathbf{z}(k+1) - \hat{\mathbf{z}}(k+1\,|\,k) \qquad (30)$$

- Updated state estimate:

$$\hat{\mathbf{x}}(k+1\,|\,k+1) = \hat{\mathbf{x}}(k+1\,|\,k) + \mathbf{W}(k+1).\mathbf{v}(k+1) \qquad (31)$$

where $\mathbf{W}(k+1)$ is called the Kalman Gain defined below in the state covariance estimation.

State covariance estimation consists of:

- State prediction covariance:

$$\mathbf{P}(k+1\,|\,k) = \begin{bmatrix} \mathbf{p}_{RR}(k+1\,|\,k) & \mathbf{p}_{R1}(k+1\,|\,k) & . & . & . & \mathbf{p}_{Rn}(k+1\,|\,k) \\ \mathbf{p}_{R1}(k+1\,|\,k) & \mathbf{p}_{11}(k+1\,|\,k) & . & . & . & \mathbf{p}_{1n}(k+1\,|\,k) \\ . & & . & . & & . \\ . & & . & & . & . \\ . & & . & & . & . \\ \mathbf{p}_{Rn}(k+1\,|\,k) & \mathbf{p}_{1n}(k+1\,|\,k) & . & . & . & \mathbf{p}_{nn}(k+1\,|\,k) \end{bmatrix} \qquad (32)$$

where $\mathbf{p}_{RR}(k+1\,|\,k)$ is calculated based on equation (9) and other elements are taken from the previous time step.

- Residual covariance or innovation covariance [33]:

$$\mathbf{S}(k+1) = \mathbf{R}(k+1) + \mathbf{H}(k+1)\mathbf{p}(k+1\,|\,k)\mathbf{H}(k+1)^T \qquad (33)$$

where $R(k+1)$ is defined in equation (24) and $H(k+1)$ is a Jacobian evaluated as:

$$\mathbf{H}(k+1) = \left.\frac{\partial \mathbf{h}(k+1)}{\partial \mathbf{x}}\right|_{\mathbf{x}=\hat{\mathbf{x}}(k+1|k)} \qquad (34)$$

- Filter Gain:

$$\mathbf{W}(k+1) = \mathbf{p}(k+1\,|\,k)\mathbf{H}(k+1)^T \mathbf{S}(k+1)^{-1} \qquad (35)$$

- Updated state covariance based on Joseph's form:

$$\mathbf{p}(k+1\,|\,k+1) = \left[\mathbf{I} - \mathbf{W}(k+1)\mathbf{H}(k+1)\right] \mathbf{p}(k+1\,|\,k) \left[\mathbf{I} - \mathbf{W}(k+1)\mathbf{H}(k+1)\right]^T \\ + \mathbf{W}(k+)\mathbf{R}(k+1)\mathbf{W}(k+1)^T \qquad (36)$$

Based on equations (25) and (26), the Jacobians of $h(k+1)$ have different forms for line and point features. For a line feature, H is calculated as:

$$H = \begin{bmatrix} H_{11} & H_{12} & H_{13} & H_{14} & H_{15} \\ H_{21} & H_{22} & H_{23} & H_{24} & H_{25} \end{bmatrix}$$

$$H_{11} = \frac{\partial \theta_{obj}}{\partial \theta} = 1$$

$$H_{12} = \frac{\partial \theta_{obj}}{\partial x} = 0$$

$$H_{13} = \frac{\partial \theta_{obj}}{\partial y} = 0$$

$$H_{14} = \frac{\partial \theta_{obj}}{\partial \varphi} = -1$$

$$H_{15} = \frac{\partial \theta_{obj}}{\partial d} = 0$$

$$H_{21} = \frac{\partial r_{obj}}{\partial \theta} = sign(A)\left(-L\cos\varphi\sin(\theta + C_2) + L\sin\varphi\cos(\theta + C_2)\right)$$

$$H_{22} = \frac{\partial r_{obj}}{\partial x} = sign(A)\cos\varphi$$

$$H_{23} = \frac{\partial r_{obj}}{\partial y} = sign(A)\sin\varphi$$

$$H_{24} = \frac{\partial r_{obj}}{\partial \varphi} = sign(A)\left(-(x + L\cos(\theta + C_2))\sin\varphi + (y + L\sin(\theta + C_2))\cos\varphi\right)$$

$$H_{25} = \frac{\partial r_{obj}}{\partial d} = -sign(A) \tag{37}$$

where A is defined as :

$$A \equiv \left(x + L\cos(\theta + C_2)\right)\cos\varphi + \left(y + L\sin(\theta + C_2)\right)\sin\varphi - d \tag{38}$$

For a point feature the Jacobian matrix, H is calculated as:

$$\mathbf{H}_{11} = \frac{\partial \theta_{obj}}{\partial \theta} = 1 - \left(\frac{1}{1 + A_4{}^2} \cdot \frac{-L\cos(\theta + C_2)A_3 - L\sin(\theta + C_2)A_2}{A_3{}^2} \right)$$

$$\mathbf{H}_{12} = \frac{\partial \theta_{obj}}{\partial x} = \frac{-1}{1 + A_4{}^2} \cdot \frac{A_2}{A_3{}^2}$$

$$\mathbf{H}_{13} = \frac{\partial \theta_{obj}}{\partial y} = \frac{-1}{1 + A_4{}^2} \cdot \frac{-1}{A_3}$$

$$\mathbf{H}_{14} = \frac{\partial \theta_{obj}}{\partial x_p} = \frac{-1}{1 + A_4{}^2} \cdot \frac{-A_2}{A_3{}^2}$$

$$\mathbf{H}_{15} = \frac{\partial \theta_{obj}}{\partial y_p} = \frac{-1}{1 + A_4{}^2} \cdot \frac{1}{A_3}$$

$$\mathbf{H}_{21} = \frac{\partial r_{obj}}{\partial \theta} = \frac{1}{2\sqrt{A_1}} \left(2L\sin(\theta + C_2)A_3 - 2L\cos(\theta + C_2)A_2 \right)$$

$$\mathbf{H}_{22} = \frac{\partial r_{obj}}{\partial x} = \frac{1}{2\sqrt{A_1}} \left(-2A_3 \right)$$

$$\mathbf{H}_{23} = \frac{\partial r_{obj}}{\partial y} = \frac{1}{2\sqrt{A_1}} \left(-2A_2 \right)$$

$$\mathbf{H}_{24} = \frac{\partial r_{obj}}{\partial x_p} = \frac{1}{2\sqrt{A_1}} \left(2A_3 \right)$$

$$\mathbf{H}_{25} = \frac{\partial r_{obj}}{\partial y_p} = \frac{1}{2\sqrt{A_1}} \left(2A_2 \right) \tag{39}$$

where A_1 to A_4 are defined as:

$$A_2 \equiv y_p - y - L\sin(\theta + C_2)$$
$$A_3 \equiv x_p - x - L\cos(\theta + C_2)$$
$$A_1 \equiv A_2{}^2 + A_3{}^2 \tag{40}$$
$$A_4 \equiv A_2 / A_3$$

A validation gate is used for association as follows:

$$e^2 = \mathbf{v}(k+1)^T \mathbf{S}(k+1)^{-1} \mathbf{v}(k+1) \le 9 \tag{41}$$

The validation gate threshold, referred to as *err_threshold* in Fig. 7, is 9 in equation (41) and the *error* that is compared to this threshold in Fig. 7 refers to *e* in equation (41).

5. Experimental Results

Experiments have been carried out in different real indoor environments. The robot *Sombrero* traveled at different speeds and collected on-the-fly range and bearing measurements using the advanced sonar ring. The sonar data were used in the off-line classification and SLAM algorithm implemented with Matlab.

5.1. A Corridor

Fig. 8 shows a corridor where the robot travels about 5 m and classifies line and point features and generates a map. Raw sonar data and the results of the proposed algorithm are shown in the figure. The map features are labeled with a sequence number and number of associations. The numbers of the associations for the line features are quite large

depending on the length of the feature. This is due to the low travel speed of 10 cm/sec and high sensing rate of 11.5 Hz. However for the point features the numbers of associations are not as large because of the limited viewing angle of the point features and weak reflections from the edges which make them invisible in some robot positions even inside their viewing angle.

5.2. Small Indoor Environment

Fig. 9 shows the outlines of the testing environment. Raw sonar data and the generated 2D map are also shown in the figure. The robot travels in a rectangular path in the small environment consisting of cardboard boxes, a wall and some lab equipment. The raw measurements contain many phantom objects which resulted from the large number of multi-path echoes due to the small size and rectangular form of the environment. Phantom objects are eliminated by ignoring echoes that have a distance of flight that is approximately an integer multiple of a nearer echo from a confirmed partial plane in the path of the phantom target. Dislocations of the walls are also due to the accumulating odometry error of the platform. However, these errors are eliminated in the generated map by applying the proposed method.
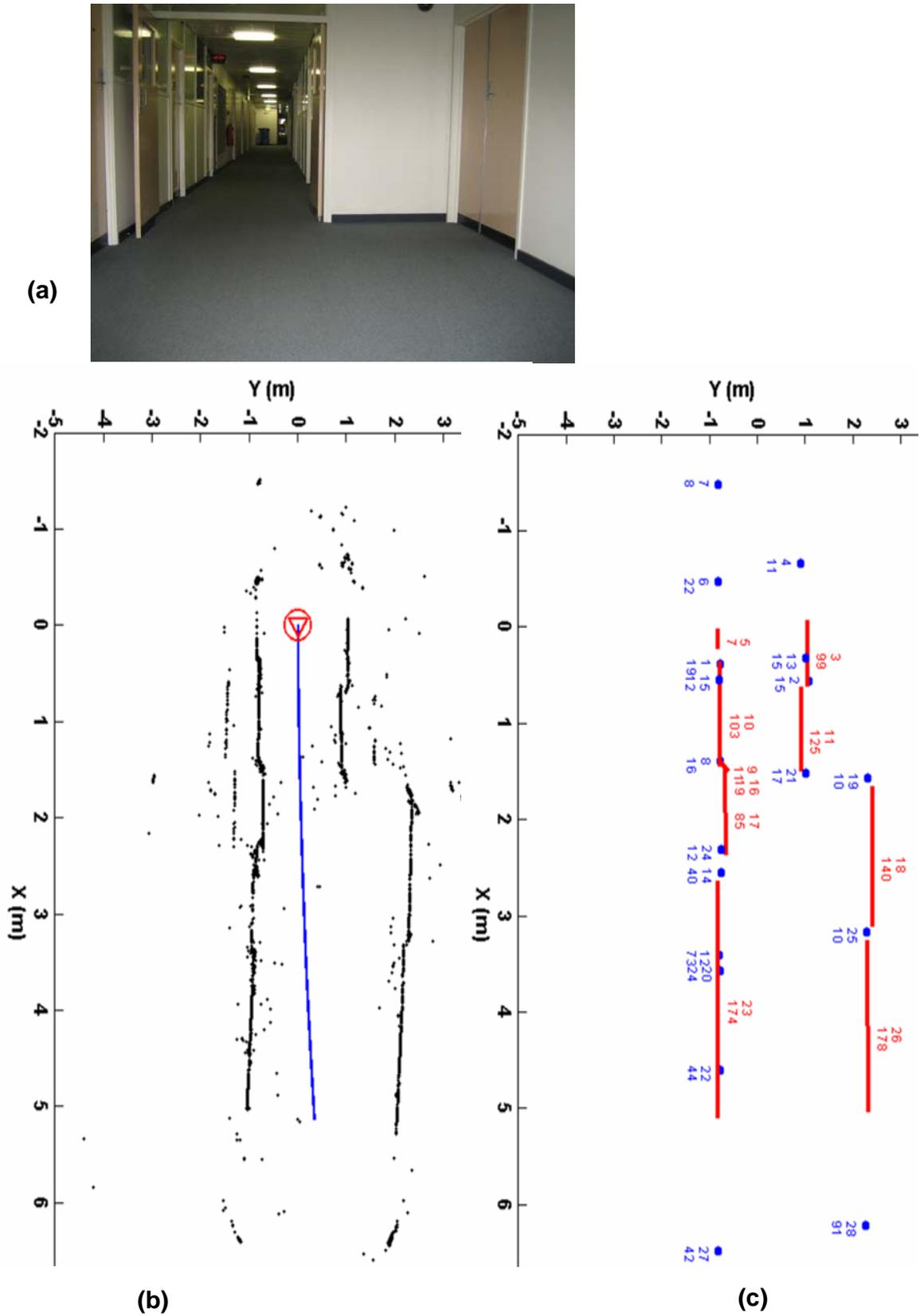
Fig. 8   (a) A Corridor where the Robot Travels About 5 m and Classifies Line and Point Features and Generates a Map. Map Features are labeled with a sequence number and the number of associations (b) the robot trajectory based on odometry and the raw sonar data (c) The map after application of SLAM EKF filtering and classification.
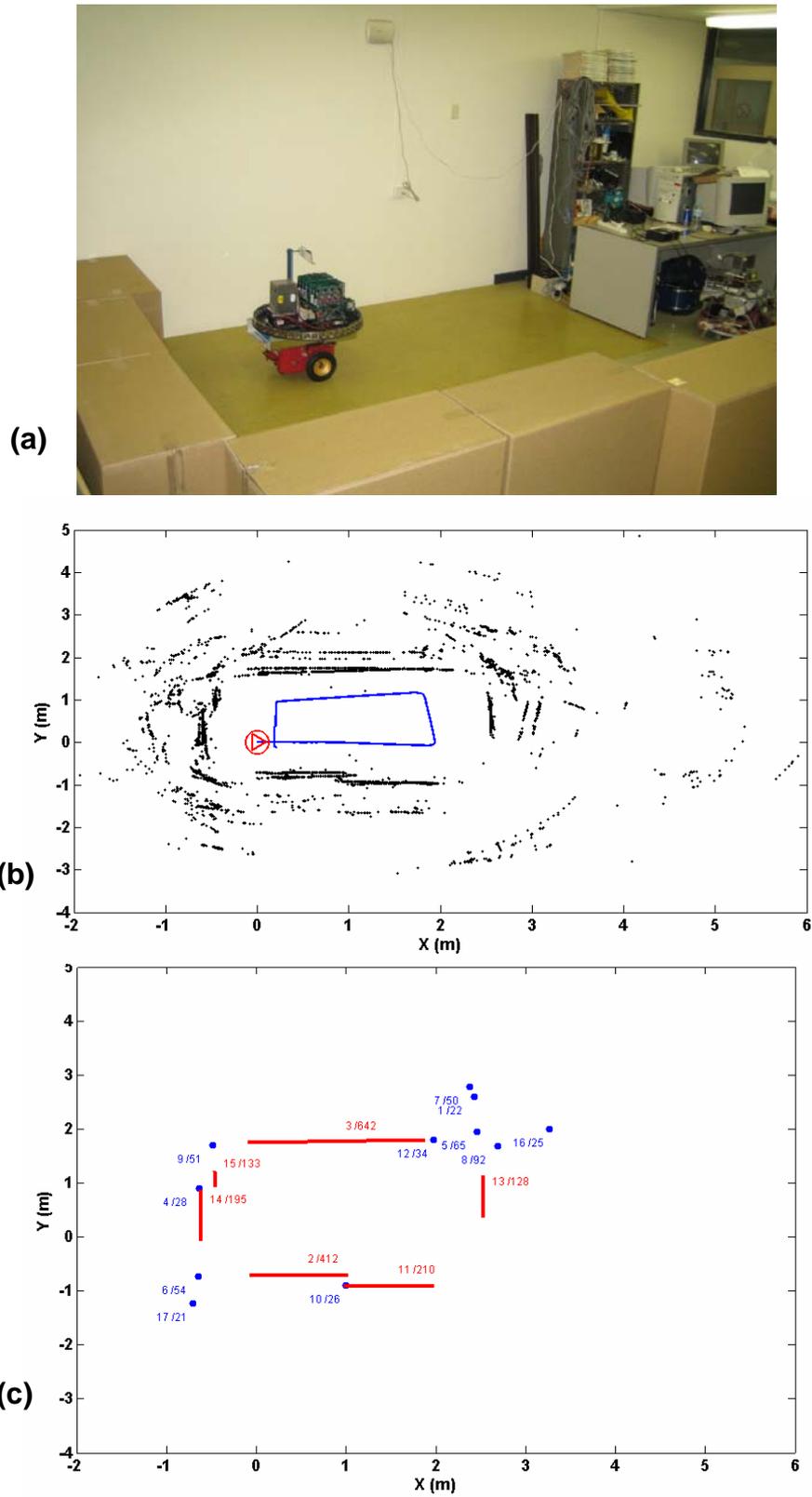
Fig. 9 (a) The robot travels in a rectangular path in the small lab environment consisting of a wall, cardboard boxes, and lab equipment (b) the robot trajectory based on odometry only and the raw sonar data (c)the SLAM map.

5.3. High-Speed Mapping

The high repetition rate of the advanced sonar ring enables the robot to travel faster while sensing the environment. The speed of the robot was set to 30 cm/sec and the experiment performed in the same corridor as in Fig. 8. The raw sonar data and the map are shown in Fig. 10. The numbers of the associations are smaller than those of Fig. 8. Some of the point features, such as number 19 and 8 in Fig. 8, have disappeared in Fig. 10. The higher speed has less effect on line features due to the very large association numbers which are still big enough even at the high speed of 30 cm/sec. Due to the limited viewing angle of the point features some of them are eliminated in high speed due to the small sensing positions and therefore small numbers of associations. However, the map generated at the speed of 30 cm/sec contains enough landmarks for navigation tasks. At higher speeds, more point features and some short line features will disappear. The execution time under Matlab for the 1511 sonar readings and 27 landmarks generated during a 17 second robot travel time was 5 seconds on a Pentium IV 2.4 GHz laptop computer. That is the processing time would allow for real time implementation for this number of landmarks and is the case in all the experiments above, however the processing time per measurement increases with the square of the number of landmarks. Reducing SLAM processing time in large scale maps is dealt with in many other research works, for example [34].
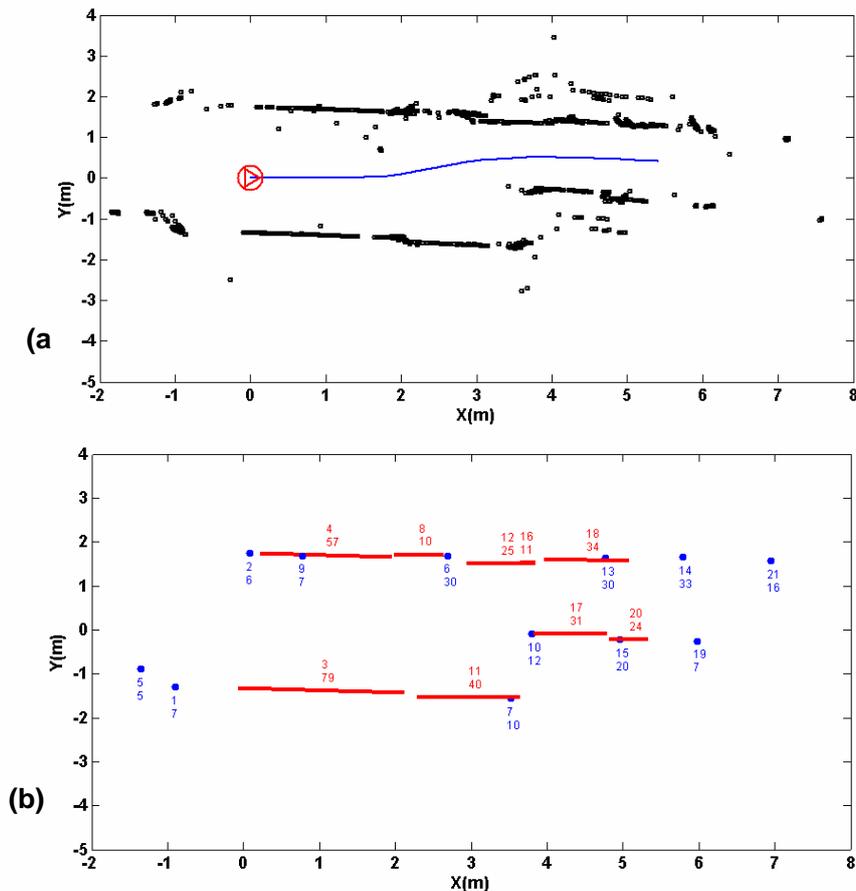

Fig. 10 A High-Speed Classification and SLAM of the Environment shown in Fig. 8(a) the Robot Trajectory and Raw Sonar Data when the Robot Travels at 30 cm/sec (b) The Map.

5.4. Map Quality

In order to show the quality of the maps, hand tape measurements of the point features in an environment are compared to the ones of a robot generated map shown in Fig 11. The point features are vertical bars of diameter 2.5 cm. The sonar ring measures the position of the bars from angles varying approximately within -45 to +45 degrees as it moves past and the map process integrates these into a single point. The measured lengths are labeled *L1* to *L14* and shown in Fig. 11. Table 5.1 presents the error in the measured lengths. The results show a small bias in that distances are overestimated in the mapping process. This effect can be attributed to an error in the speed of sound.
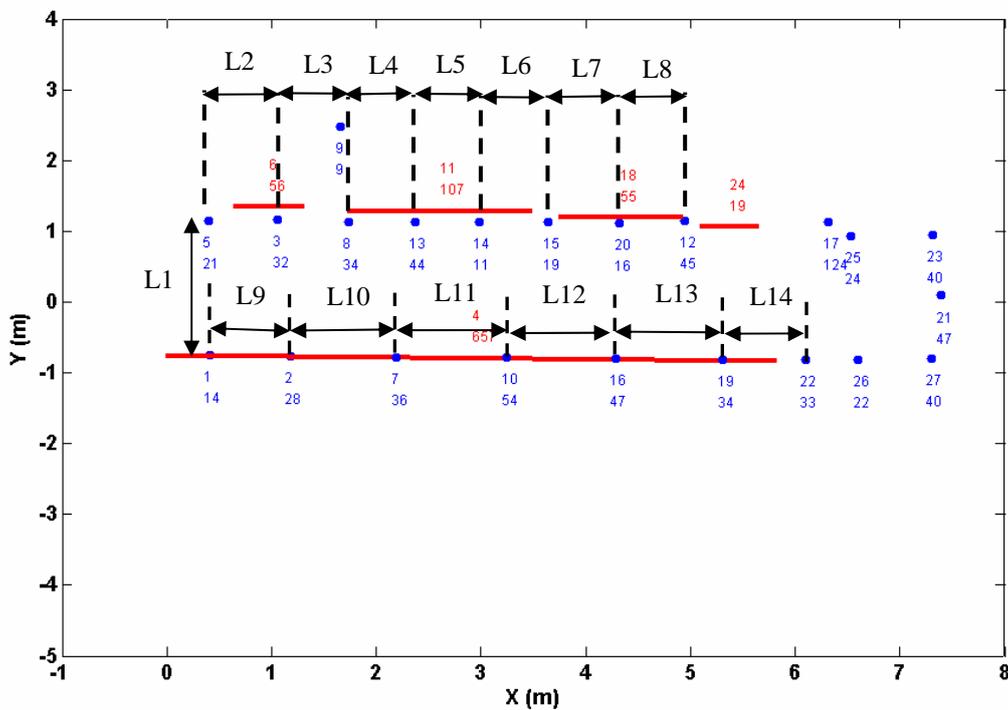

Fig. 11 Generated Map of the Corridor as in section 5.5.3

Table 1 Errors in Map Generation

	L1	**L2**	**L3**	**L4**	**L5**	**L6**	**L7**
Map Value(cm)	190.3	65.4	65.9	63	61.6	65.4	62.9
Real Value(cm)	189.5	64.5	64	62.6	62.1	64.5	62.6
Error (cm)	0.8	0.9	1.9	0.4	-0.5	0.9	0.3
	L8	**L9**	**L10**	**L11**	**L12**	**L13**	**L14**
Map Value(cm)	64	76.6	101.4	102.6	102.1	101.7	77.2
Real Value(cm)	65.1	76.4	101.2	101.2	101.2	101.2	76.7
Error (cm)	-1.1	0.2	0.2	1.4	0.9	0.5	0.5

6. Conclusions and Future Work

This paper has presented a novel approach to feature classification within the SLAM process using a recently developed advanced sonar ring. The advanced sonar ring produces accurate measurements and allows reliable measurement association with map features. The error in range measurement has been measured as less than 0.6mm and for bearing angle is less than 0.17 degrees [29]. The proposed algorithm produces high quality sonar maps with a Kalman filter SLAM approach. This work highlights the benefit of accurate sonar measurements in robust feature classification using a fast hypothesis generation and verification technique. The performance of the algorithm has been illustrated by experimental results.

The system described in this paper allows reliable measurement association with map features. However failure can rarely occur due to erroneous associations when odometry errors exceed expectations, and errors occur in the generation of probational features.

The advanced sonar ring senses the environment at the high repetition rate of 11.5 Hz without mechanical problems and delays associated with scanning sonar sensors as in [7,16]. As a result, this system has the advantage of providing high-density maps which enable the robot to travel faster (30 cm/sec) compared to previous works [7,16,19,21]. However, in previous works, object classification is performed in one sensing cycle which is not the case for the advanced sonar ring. This is due to the sensor design which employs one transmitter per pair. To enable the sensor to classify objects in each measurement cycle, each direction must contain at least two transmitters and two receivers [30,35]. To reduce the cost and complexity, the sensor design was planned based on in-movement-classification. This paper has presented a novel delayed classification algorithm which categorizes features within the SLAM process. The method is capable of

classifying the objects within a short distance of travel of about 10 cm. The main advantage of the proposed system is enabling the robot to travel faster while providing dense maps of the indoor environment.

Future work will concentrate on the real time implementation of the algorithm on *Sombrero*, improving association and recovering from failure of SLAM. The related problems of kidnapping, loop closure, large-scale SLAM and a map matching strategy to re-establish robot's position when its uncertainty is too large will also be investigated.

Acknowledgements

References

[1] L. Kleeman,"*Fast and accurate sonar trackers using double pulse coding",1999 IEEE/RSJ International Conference on Intelligent Robots and Systems (IROS'99): Human and Environment Friendly Robots whith High Intelligence and Emotional Quotients', Oct 17-Oct 21 1999*, Kyongju, South Korea, 1999 (IEEE, Piscataway, NJ, USA), p. 1185-1190.

[2] R. Kuc and V. B. Viard,"Physically based navigation strategy for sonar-guided vehicles", *International Journal of Robotics Research* **10,** 75-87 (1991).

[3] D. Murray and C. Jennings,"*Stereo vision based mapping and navigation for mobile robots",Proceedings of the 1997 IEEE International Conference on Robotics and Automation, ICRA. Part 2 (of 4), Apr 20-25 1997*, Albuquerque, NM, USA, 1997 (IEEE, Piscataway, NJ, USA), p. 1694-1699.

[4] C. Schroeter, H.-J. Boehme, and H.-M. Gross,"*Robust map building for an autonomous robot using low-cost sensors",2004 IEEE International Conference on Systems, Man and Cybernetics, SMC 2004, Oct 10-13 2004*, The Hague, Netherlands, 2004 (Institute of Electrical and Electronics Engineers Inc., New York, NY 10016-5997, United States), p. 5398-5403.

[5] T. Yata, L. Kleeman, and S. i. Yuta,"Fast-bearing measurement with a single ultrasonic transducer", *International Journal of Robotics Research* **17,** 1202-1213 (1998).

[6] A. Davison, *Mobile Robot Navigation using Active Vision* (D.Phil Thesis University of Oxford, 1998).

[7] A. Diosi and L. Kleeman,"*Advanced sonar and laser range finder fusion for simultaneous localization and mapping",2004 IEEE/RSJ International Conference on Intelligent Robots and Systems (IROS), Sep 28-Oct 2 2004*, Sendai, Japan, 2004 (Institute of Electrical and Electronics Engineers Inc., New York, NY 10016-5997, United States), p. 1854-1859.

[8] M.-H. Li, B.-R. Hong, and R.-H. Luo,"Simultaneous localization and map building for mobile robot", *Harbin Gongye Daxue Xuebao/Journal of Harbin Institute of Technology* **36,** 874-876 (2004).

[9] A. Grossmann and R. Poli,"Robust mobile robot localisation from sparse and noisy proximity readings using Hough transform and probability grids", *Robotics and Autonomous Systems* **37,** 1-18 (2001).

[10] R. Gartshore, A. Aguado, and C. Galambos,"*Incremental Map Building using an Occupancy Grid for an Autonomous Monocular Robot",Proceedings of the 7th International Conference on Control, Automation, Robotics and Vision, ICARC 2002, Dec 2-5 2002*, Singapore, Singapore, 2002 (Nanyang Technological University), p. 613-618.

[11] J. J. Leonard, H. F. Durrant-Whyte, and I. J. Cox,"Dynamic map building for an autonomous mobile robot", *International Journal of Robotics Research* **11,** 286-298 (1992).

[12] D. Maksarov and H. Durrant-Whyte,"Mobile vehicle navigation in unknown environments: a multiple hypothesis approach", *IEE Proceedings: Control Theory and Applications* **142,** 385-400 (1995).

[13] T. Tsubouchi,"*Nowadays trends in map generation for mobile robots",Proceedings of the 1996 IEEE/RSJ International Conference on Intelligent Robots and Systems, IROS. Part 2 (of 3), Nov 4-8 1996*, Osaka, Jpn, 1996 (IEEE, Piscataway, NJ, USA), p. 828-833.

[14] K.-T. Song and C. C. Chang,"*Ultrasonic sensor data fusion for environment recognition",Proceedings of the IEEE/RSJ International Conference on Intelligent Robots and Systems, Jul 26-30 1993*, Yokohama, Jpn, 1993 (Publ by IEEE, Piscataway, NJ, USA), p. 384-390.

[15] K. S. Chong and L. Kleeman,"Feature-based mapping in real, large scale environments using an ultrasonic array", *International Journal of Robotics Research* **18,** 3-19 (1999).

16   L. Kleeman,"*Advanced Sonar and Odometry Error Modeling for Simultaneous Localisation and Map Building*",*2003 IEEE/RSJ International Conference on Intelligent Robots and Systems, Oct 27-31 2003*, Las Vegas, NV, United States, 2003 (Institute of Electrical and Electronics Engineers Inc.), p. 699-704.

17   J. Leonard, J. and H. Durrant-Whyte, F., "Simultaneous map building and localization for an autonomous mobile robot," Report No. 0499-9320 (1990).

18   O. Wijk and H. I. Christensen,"Triangulation-based fusion of sonar data with application in robot pose tracking", *IEEE Transactions on Robotics and Automation* **16,** 740-752 (2000).

19   W. D. Rencken,"*Autonomous sonar navigation in indoor, unknown and unstructured environments*",*Proceedings of the IEEE/RSJ/GI International Conference on Intelligent Robots and Systems. Part 1 (of 3), Sep 12-16 1994*, Munich, Ger, 1994 (IEEE, Piscataway, NJ, USA), p. 431-438.

20   G. Zunino and H. I. Christensen,"*Simultaneous localization and mapping in domestic environments*",*International Conference on Multisensor Fusion and Integration for Intelligent Systems, Aug 20-22 2001*, Baden-Baden, 2001 (Institute of Electrical and Electronics Engineers Inc.), p. 67-72.

21   K. S. Chong and L. Kleeman,"Mobile-robot map building from an advanced sonar array and accurate odometry", *International Journal of Robotics Research* **18,** 20-36 (1999).

22   A. Heale and L. Kleeman,"*A real time DSP sonar echo processor*",*2000 IEEE/RSJ International Conference on Intelligent Robots and Systems, Oct 31-Nov 5 2000*, Takamatsu, 2000 (Institute of Electrical and Electronics Engineers Inc.), p. 1261-1266.

23   H. J. Jeon and B. K. Kim,"*Study on world map building for mobile robots with tri-aural ultrasonic sensor system*",*Proceedings of the 1995 IEEE International Conference on Robotics and Automation. Part 3 (of 3), May 21-27 1995*, Nagoya, Jpn, 1995 (IEEE, Piscataway, NJ, USA), p. 2907-2912.

24   J. Howell and B. R. Donald,"*Practical mobile robot self-localization*",*ICRA 2000: IEEE International Conference on Robotics and Automation, Apr 24-Apr 28 2000*, San Francisco, CA, USA, 2000 (Institute of Electrical and Electronics Engineers Inc., Piscataway, NJ, USA), p. 3485-3492.

25   J. M. P. Lorenzo, R. Vazquez-Martin, P. Nunez, E. J. Perez, and F. Sandoval,"*A hough-based method for concurrent mapping and localization in indoor environments*",*2004 IEEE Conference on Robotics, Automation and Mechatronics, Dec 1-3 2004*, Singapore, 2004 (Institute of Electrical and Electronics Engineers Inc., New York, NY 10016-5997, United States), p. 840-845.

26   R.-H. Luo and B.-R. Hong,"Simultaneous localization and mapping based on multisensor fusion", *Harbin Gongye Daxue Xuebao/Journal of Harbin Institute of Technology* **36,** 566-569 (2004).

27   W. Niblack and D. Petkovic,"On improving the accuracy of the Hough transform", *Machine Vision and Applications* **3,** 87-106 (1990).

28   X. Yun, K. Latt, and J. S. Glennon,"*Mobile robot localization using the Hough transform and neural networks*",*Proceedings of the 1998 IEEE International Symposium on Intelligent Control, ISIC, Sep 14-17 1998*, Gaithersburg, MD, USA, 1998 (IEEE, Piscataway, NJ, USA), p. 393-400.

29   S. Fazli and L. Kleeman,"Sensor Design and Signal processing for an Advanced Sonar Ring", *Accepted for Publication, Robotica Journal, Cambridge University Press* (2005).

30   L. Kleeman and R. Kuc,"Mobile robot sonar for target localization and classification", *International Journal of Robotics Research* **14,** 295-318 (1995).

31   S. Fazli and L. Kleeman,"*A Low Sample Rate Real Time Advanced Sonar Ring*",*2004 Australasian Conference on Robotics and Automation, Dec 6-8 2004*, Canberra,Australia, 2004.

32   S. Fazli and L. Kleeman,"*A Real Time Advanced Sonar Ring with Simultaneous Firing*",*2004 IEEE/RSJ International Conference on Intelligent Robots and Systems, Sep 28-Oct 2 2004*, Sendai, Japan, 2004, p. 1872-1877.

33   Y. Bar-Shalom, X. Rong Li, and T. Kirubarajan, *Estimation with Applications to Tracking and Navigation [electronic resource]*, 1st ed. (Wiley-Interscience, 2001).

34   M. Bosse, P. Newman, J. Leonard, and S. Teller,"Simultaneous localization and map building in large-scale cyclic environments using the atlas framework", *International Journal of Robotics Research* **23,** 1113-1139 (2004).

35   L. Kleeman and R. Kuc,"*Optimal sonar array for target localization and classification*",*Proceedings of the 1994 IEEE International Conference on Robotics and Automation, May 8-13 1994*, San Diego, CA, USA, 1994 (Publ by IEEE, Piscataway, NJ, USA), p. 3130-3135.